International Journal of Heat and Mass Transfer 51 (2008) 6077–6089

Contents lists available at ScienceDirect

International Journal of Heat and Mass Transfer

journal homepage: www.elsevier.com/locate/ijhmt

Numerical investigations on flow behaviour and energy separation in Ranque–Hilsch vortex tube

Upendra Behera [a], P.J. Paul [b], K. Dinesh [a], S. Jacob [a,*]

[a] Centre for Cryogenic Technology, Indian Institute of Science, Bangalore 560 012, India
[b] Department of Aerospace Engineering, Indian Institute of Science, Bangalore 560 012, India

ARTICLE INFO

Article history:
Received 3 September 2007
Received in revised form 24 March 2008
Available online 16 June 2008

Keywords:
Ranque–Hilsch vortex tube
CFD simulation
Fluid properties
Stagnation point
Energy separation

ABSTRACT

A three-dimensional numerical model of Ranque–Hilsch vortex tube has been developed using the commercial CFD code (Star-CD) to analyze the flow parameters and energy separation mechanism inside the tube. Investigations have been done on the variation of fluid properties and flow parameters as the fluid particles progress in the flow field by tracking different particles exiting through the hot and cold end. Fluid properties like stagnation temperature, static temperature, static pressure and total pressure and flow parameters like axial, radial and swirl velocities are obtained along the axial and radial directions to understand the flow behaviour inside the tube. The presence of free vortex zone inside the tube also has been investigated. Possible energy transfer mechanisms are discussed and an estimate has been made on the magnitude of energy transfer from the cold end exit flow to hot end exit flow. Effects of secondary circulation and length of the tube on energy separation also have been evaluated.

1. Introduction

Vortex tube known also as Ranque–Hilsch tube was invented by Ranque [1] in 1933, while it was analyzed by Hilsch [2] in 1947. The flow of any fluid rotating about an axis is called a vortex. In the vortex tube, the vortex motion is created by tangential injection of a compressed fluid, which separates into two streams, one hot and the other cold. When compressed gas is injected through one or more tangential nozzle(s) into a scroll chamber, a strong circular flow field is established, giving rise to a non-uniform temperature field. The gas layers closer to the axis are cooler than the incoming feed gas and the peripheral layers of the gas are hotter. In a counter flow vortex tube, a fraction of the feed gas exits as cold core flow at the central zone of one end of the tube through an orifice and the balance fraction of flow exits as hot peripheral flow at the opposite end through a throttle valve. A large number of investigators up to now have postulated that the peripheral hot stream is a free vortex in which the angular velocity increases with decreasing radius and the inner cold stream is a forced vortex where the angular velocity is proportional to the radial distance.

Many theories [3–5] postulated to explain the temperature separation of the flow in the vortex tube, have a weak link and are not able to convincingly explain the mechanism of energy separation taking place between the core and the peripheral flows in the vortex tube. Also, several numerical investigations [6–9] by using various numerical models have been conducted to understand the flow behaviour and the energy separation mechanism in Ranque–Hilsch vortex tube. No exact theory has come up till today. The work reported here is an attempt to use CFD analysis to provide a clear insight into these mechanisms.

2. Numerical modeling

A three-dimensional numerical model of the Ranque–Hilsch vortex tube has been developed using code system of Star-CD (finite volume approach developed by Computational Dynamics Ltd.). The program has the provision for solving compressible and turbulent flows. The conservation equations used for mass and momentum in Cartesian coordinate (Star-CD Methodology and User Guide [10]) are as below.

$$\frac{\partial}{\partial t}(\rho) + \frac{\partial}{\partial x_j}(\rho u_j) = S_m \tag{1}$$

$$\frac{\partial}{\partial t}(\rho u_i) + \frac{\partial}{\partial x_j}(\rho u_j u_i - \tau_{ij}) = -\frac{\partial P}{\partial x_i} + S_i \tag{2}$$

Considering high velocity (close to Mach 1) and compressible fluid flow, the total enthalpy equations have been solved.

$$\frac{\partial}{\partial t}(\rho H) + \frac{\partial}{\partial x_j}(\rho u_j H - F_{h,j} - u_i \tau_{ij}) = \frac{\partial P}{\partial t} + S_i u_i + S_h \tag{3}$$

where, $H = h + \frac{1}{2}u_i^2$.

The flow in the vortex tube is assumed to be steady and periodic. The working fluid (air) has been modeled as ideal gas where

* Corresponding author. Tel.: +91 80 22933077; tel./fax: +91 80 23601612.
E-mail address: jacob@ccf.iisc.ernet.in (S. Jacob).

0017-9310/$ - see front matter © 2008 Elsevier Ltd. All rights reserved.
doi:10.1016/j.ijheatmasstransfer.2008.03.029

Nomenclature

A	tube cross-sectional area
C_p	specific heat of air assumed to be constant and equal to1.005 kJ/kg K
d	diameter
D	diameter of vortex tube
dT	temperature gradient across the control volume boundary
dv	axial velocity difference across the control volume boundary
dx	finite distance of cell centroids on either side of boundary normal to the boundary surface
$F_{h,j}$	diffusion thermal energy flux in *xi*-direction
h	static enthalpy
H	total enthalpy
K	thermal conductivity
K_{eff}	effective thermal conductivity ($=K+K_t$)
k	turbulence kinetic energy
L	length of the vortex tube
M	Mach number
m	mass flow rate
P	piezometric pressure
P_r	Prandtl number taken close to unity (0.9)
Q	heat flux
r	radius
r_b	radial distance of control volume boundary from the axis
S_i	momentum source components
S_h	energy source
S_m	mass source
T	temperature
t	time
u	swirl velocity (m s^{-1})
u_i	fluid velocity component in *xi*-direction
v	radial velocity
w	axial velocity
W	work
xi	cartesian coordinate ($i=1, 2, 3$)

Greek symbols

β	coefficient used in Eq. (5)
ε	turbulence dissipation rate
η_0	coefficient used in Eq. (5)
γ	specific heat ratio
μ	dynamic viscosity
ω	angular velocity
ρ	density
ψ	stream function
τ_{ij}	stress tensor components
τ	shear stress
θ	angle

Subscripts

c	cold gas
h	hot gas
i	inlet in vortex tube
t	turbulent
st	static

$\rho = f(T,P)$. Molecular viscosity, specific heat and thermal conductivity are considered to be constant. Prandtl number is taken as constant and close to unity ($P_r = 0.9$).

The RNG k–ε turbulent model in conjunction with law of the wall function is employed to account for turbulence. This model uses RNG (Re-normalization group) methodology of Yakhot and Orszag [11] for the governing equation of turbulence and model coefficients have been revalued. This model accounts the effect of swirl on the turbulent intensity and calculates, rather than assumes, a turbulent Prandtl number [7].

The equations involved in RNG k–ε model for turbulence energy and turbulence dissipation rate [10] with standard notations are given as

$$\frac{\partial}{\partial t}(\rho k)+\frac{\partial}{\partial x_j}\left(\rho\tilde{u}_j k-\frac{\mu_{\text{eff}}}{\sigma_k}\frac{\partial k}{\partial x_j}\right) = \mu_t(P+P_B)-\rho\varepsilon-\frac{2}{3}\left(\mu_t\frac{\partial u_i}{\partial x_i}+\rho k\right)\frac{\partial u_i}{\partial x_i} \tag{4}$$

$$\frac{\partial}{\partial t}(\rho\varepsilon)+\frac{\partial}{\partial x_j}\left(\rho\tilde{u}_j\varepsilon-\frac{\mu_{\text{eff}}}{\sigma_\varepsilon}\frac{\partial\varepsilon}{\partial x_j}\right) = C_{\varepsilon1}\frac{\varepsilon}{k}\left[\mu_t P-\frac{2}{3}(\mu_t\frac{\partial u_i}{\partial x_i}+\rho k)\frac{\partial u_i}{\partial x_i}\right] + C_{\varepsilon3}\frac{\varepsilon}{k}\mu_t P_B-C_{\varepsilon2}\rho\frac{\varepsilon^2}{k} + C_{\varepsilon4}\rho\varepsilon\frac{\partial u_i}{\partial x_i}-\frac{C_\mu\eta^3(1-\eta/\eta_0)}{1+\beta\eta^3}\frac{\rho\varepsilon^2}{k} \tag{5}$$

where

$C_{\varepsilon1}$, $C_{\varepsilon2}$, $C_{\varepsilon3}$ and $C_{\varepsilon4}$ are co-efficients and given by 1.42, 1.68, 0.0 or 1.42 (if $P_B > 0$ and 0 otherwise) and −0.387, respectively. C_μ, η_0, σ_ε, σ_k, σ_h and β are empirical coefficients usually taken as constants. S_{ij} is element of mean strain and is twice of s_{ij}.

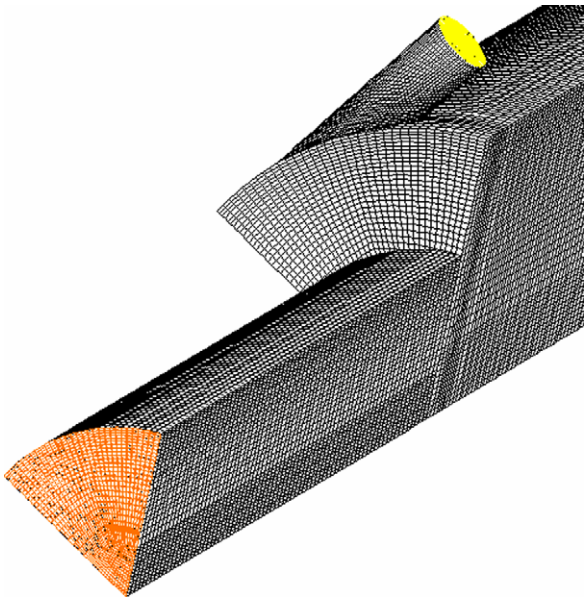

Fig. 1. Three-dimensional model of vortex tube in 60° sector.

$$\mu_{\text{eff}} = \mu+\mu_t$$

$$P \equiv 2s_{ij}\frac{\partial u_i}{\partial x_j},\quad P_B=-\frac{g_i}{\sigma_h}\frac{1}{\rho}\frac{\partial\rho}{\partial x_i},\quad \eta\equiv Sk/\varepsilon,\quad s\equiv(2s_{ij}s_{ij})^{1/2},$$

$$\eta_0=4.38,\quad \beta=0.012.\quad C_\mu=0.085,\quad \sigma_\varepsilon=0.719,\quad \sigma_k=0.719,$$

$$\sigma_h=0.9.$$

In the present studies we could not use LES model due to convergence problems. Otherwise LES model could have captured transient flow patterns and temperature separation in Ranque–Hilsch vortex tube. Farouk et al. [12] have successfully used the LES techniques to predict the flow field and the temperature separation more accurately as compared to k–ε model and could show small vortices in the core flow regime in Ranque–Hilsch vortex tube. The temperature separation predicted by LES model is in good agreement with the numerical and experimental results by Skye et al. [8].

The geometry of the model is identical to the vortex tube used for experiments [13]. Optimized parameters for a 12 mm diameter counter flow vortex tube used in the analysis are,

$L/D = 30$, $d_c = 7$ mm, $A_i/A = 0.07$
Number of nozzles = 6 (convergent)

The boundary conditions are derived from experimental measurements at respective locations of the vortex tube. Dry and oil free air is supplied to the vortex tube with a stagnation pressure of 0.55 MPa (absolute) and total temperature of 300 K at the nozzle inlet. Hot and cold end outlets are applied with pressure boundary condition measured from the experiments. Adiabatic walls are used with no-slip conditions. Axi-symmetric flow assumption may not be appropriate for vortex tube having finite number of nozzles. As the flow inside the tube is periodic having six numbers of convergent nozzles, a 60° sector is modeled with cyclic boundary conditions as shown in Fig. 1. 3D modeling of the vortex tube will eliminate the errors in the estimation of velocity components at the inlet and exit locations and the area of air inlet. Hexahedral meshes consisting of 0.89 million cells with refinement at inlet, outlet and wall are used for the analysis. Mesh dependency study shows no appreciable changes in results beyond this mesh density [13].

3. Flow analysis

CFD analysis has been done to investigate the variation of static and total temperatures, static and total pressures as well as

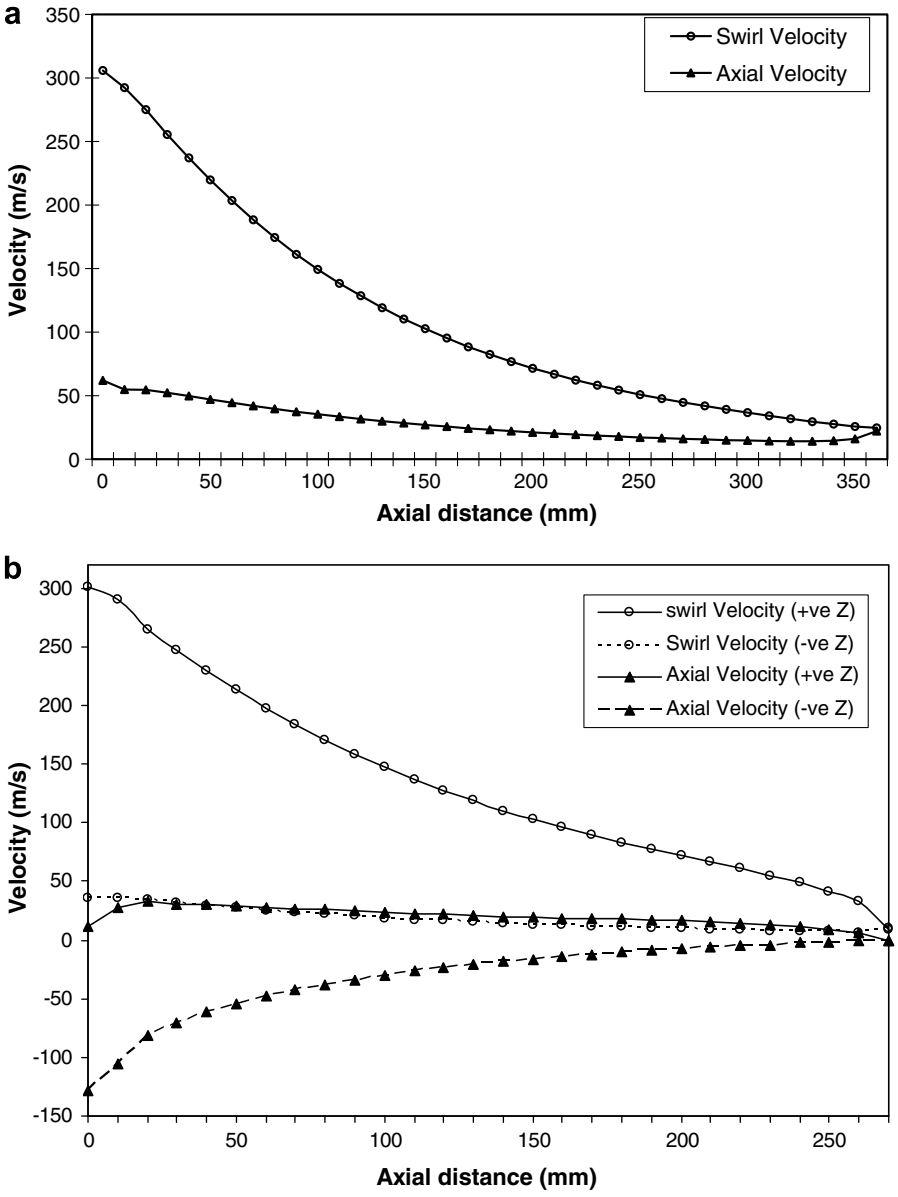

Fig. 2. Velocity components of the tracked particle as it progresses in flow field: (a) particle exiting through hot end, (b) particle exiting through cold end after flow reversal (+ve Z: particle moving in +ve Z-direction, −ve Z: particle moving in −ve Z-direction).

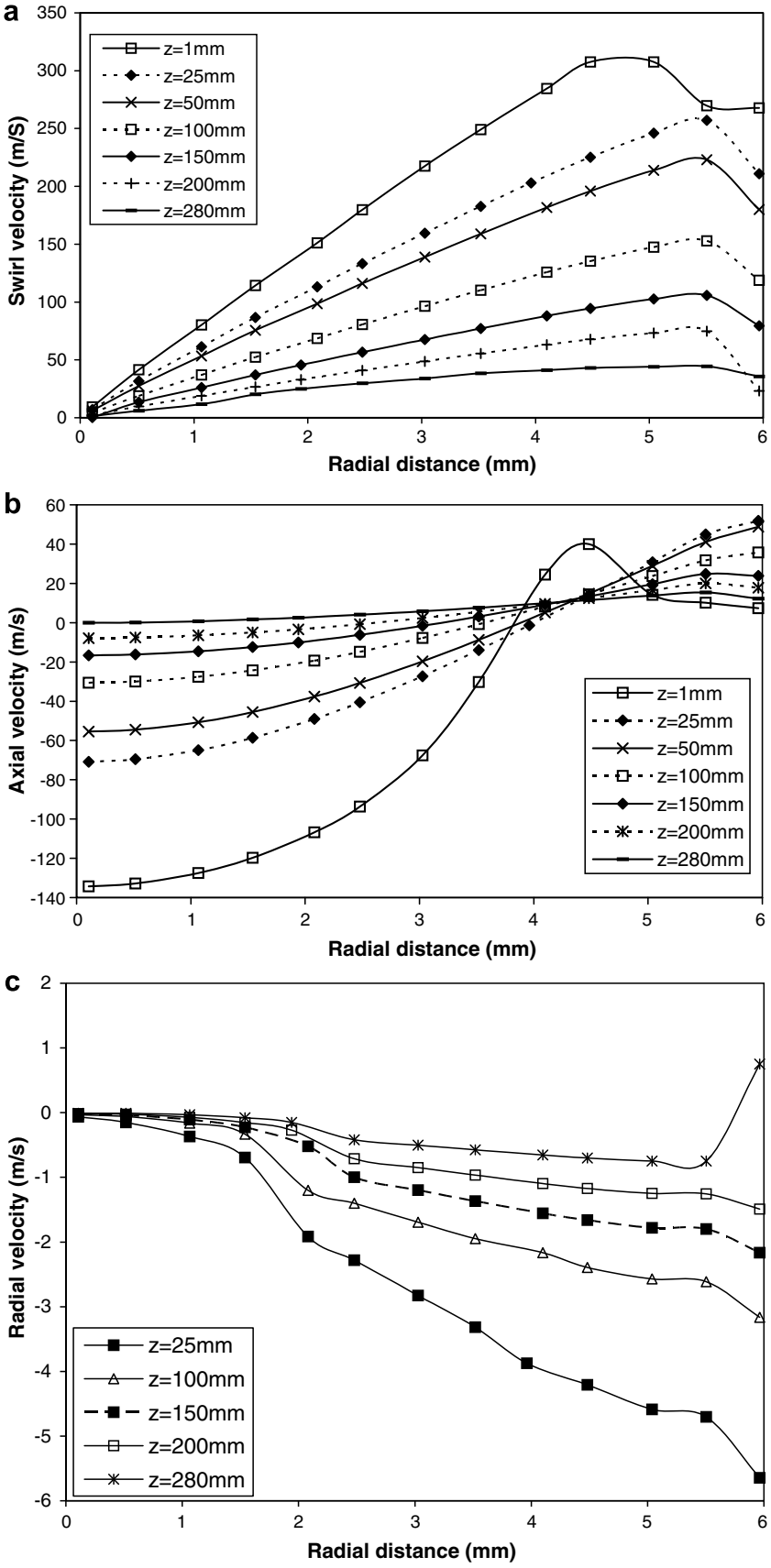

Fig. 3. Radial profile of velocity components: (a) swirl velocity, (b) axial velocity and (c) radial velocity.

the velocity components of the particle as it progresses in the flow field, starting from the entry through nozzle to the exit by tracking the particles to understand the flow phenomenon inside the vortex tube. Vortex tube with L/D ratio of 30 has been considered for

analysis where the stagnation point lies within the tube length [13].

3.1. Velocity components

The variation of axial and swirl velocity components for typical particles exiting through hot and cold end after flow reversal near stagnation point are shown in Fig. 2. Both velocity components of the particle decrease gradually as it moves on to hot end exit as shown in Fig. 2a. Swirl velocity has much higher magnitude (300 m/s) than axial (55 m/s) at the inlet zone but decreases rapidly as the particle progresses towards the hot end. Fig. 2b shows the variation of the axial and swirl velocity for the particles which move along with hot end particles till stagnation point and exits through cold end. It is observed that both the velocity components vary similar to the particles exiting through hot end. The drag force caused by the difference of pressure between flow field and cold end exit will continuously act on particles moving towards the hot end. When the particle is not left with any momentum to flow against this pressure gradient, its axial velocity ceases to zero and later on reverse its direction of flow, by moving towards the cold end exit. Further acted by the differential pressure, the particle expands causing to considerable increase in axial velocity in negative direction.

Variation of velocity components along radial direction are shown in Fig. 3a–c. As shown in Fig. 3a, the variation of swirl velocity along the radial direction does not show any conclusive evidence of the existence of free vortex zone inside the tube except near the inlet zone. The same has been verified and found to be so even for bigger diameter (D = 24 mm) vortex tube as shown in Fig. 4. Most of the flow inside the tube is governed by forced vortex regime where the swirl velocity is proportional to the radius. Fig. 3b shows the axial velocity magnitude and the thickness of both the flow regions (in radial direction) moving in opposite direction. Thickness of cold end exit region comes to zero at axial distance of 280 mm from inlet, which is the stagnation point. Radial velocity represented in Fig. 3c is very small in magnitude. Particles at all cross-sections are moving towards the axis expanding from high to low-pressure zone.

3.2. Pressure components

Variation of static and total pressure of two particles, first one exiting through hot end and the second through cold end after flow reversal have been plotted in Fig. 5. Total pressure of the particle varies similar to that of velocity as it moves to the hot end exit and the static pressure variation is minimal. Most of the expansion takes place within the nozzle, where the static pressure drops from inlet pressure of 5.5 bar to about 2.7 bar, leading to near sonic velocity of the particle. Static pressure does not change much thereafter along the tube till hot end.

The cold end exiting particle expands similar to hot end exiting particle till it reaches stagnation point. After flow reversal the particle further expands from 2.2 bar at stagnation point to nearly atmospheric pressure at cold end exit leading to increase in negative axial velocity. Total pressure matches to static pressure during reverse flow but attains a higher value than static pressure towards exit due to increase in velocity.

Static pressure increases along radial direction at all Z cross-sections as shown in Fig. 6, leading to negative radial velocity of the particle as shown in Fig. 3. Difference of pressure between peripheral layers to core layers decreases with increasing axial distance from inlet.

3.3. Temperature components

Temperature profile of the particle as it moves on from inlet to hot end exit has been illustrated in Fig. 7a. Static temperature at the nozzle exit drops down to 255 K from 300 K at the inlet as a result of isentropic expansion of the particle in nozzle from 5.5 bar to 2.7 bar. This is the lowest static temperature in vortex tube. As particle progresses towards hot end, it gains thermal energy and temperature increases. Most of the energy interaction takes place within its initial 10D length of the tube. Small increase in temperature is noticed beyond this length. Static temperature slowly catches the total temperature curve as the velocity of the particle reduces gradually towards hot end exit because of the conversion of kinetic energy into thermal energy by the action of viscous shear.

As illustrated in Fig. 7b, even the particles exiting through the cold end follow the same trend of temperature increase during its flow towards stagnation point i.e temperature increases along the tube length. Temperature of this particle drops drastically after flow reversal, loosing its energy to peripheral particles on its travel to cold end exit.

A closer look at the static temperature plot gives an insight to the cause of radial heat transfer. It can be seen from Fig. 7b that

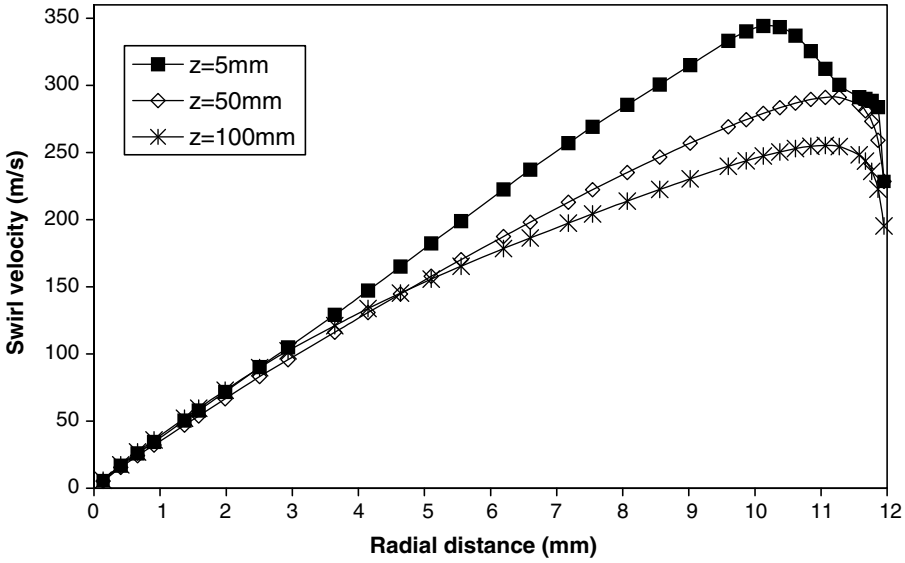

Fig. 4. Radial profile of swirl velocity for 24 mm diameter vortex tube.

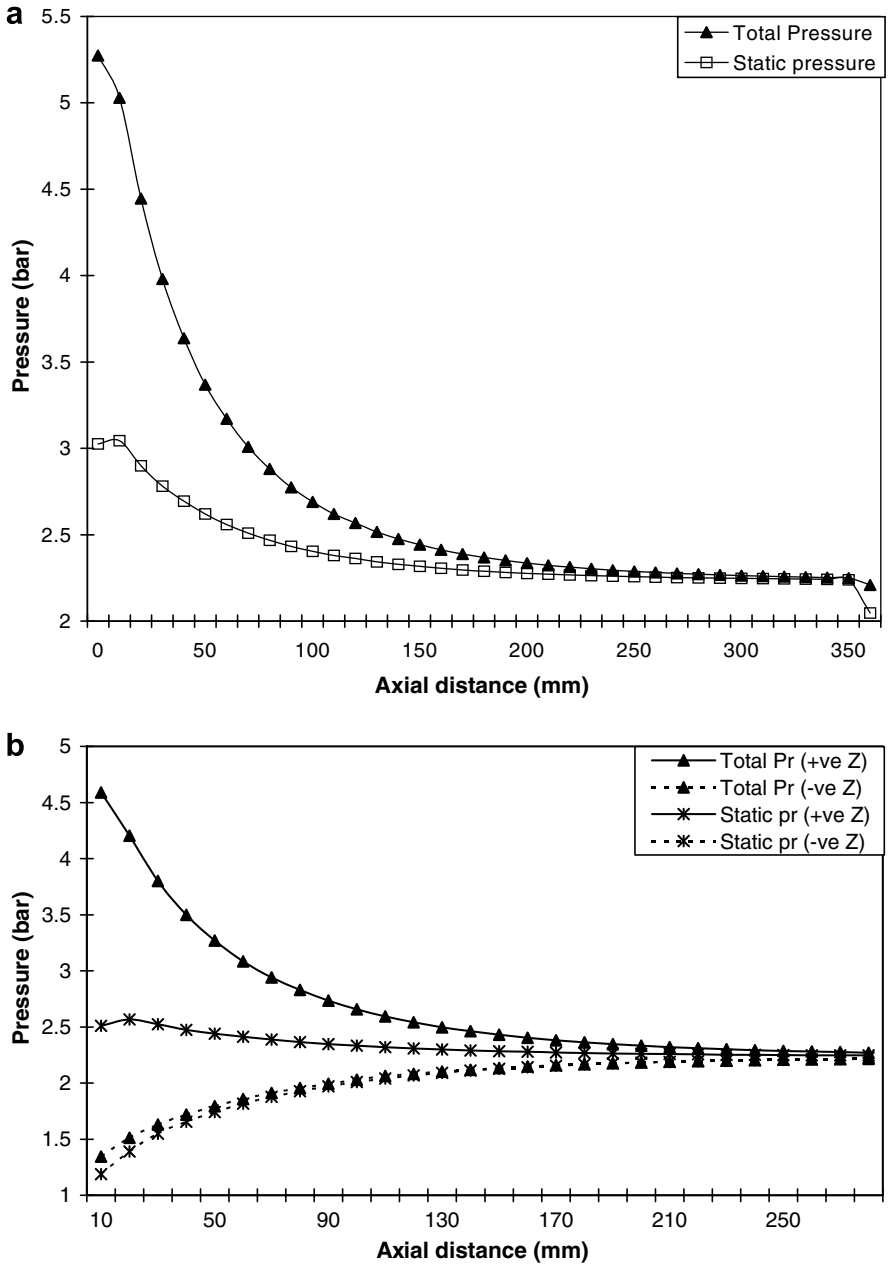

Fig. 5. Pressure of the tracked particle as it progresses in flow filed: (a) particle exiting through hot end, (b) particle exiting through cold end after flow reversal (+ve Z: particle moving in +ve Z-direction, −ve Z: particle moving in −ve Z-direction).

the static temperature of particle moving towards stagnation point is less than the static temperature on its way back to cold end exit at the same Z cross-section. Though the total temperatures of peripheral layers are higher than core layers, the static temperature is less due to higher kinetic energy part in it. Total temperature of a compressible fluid is represented by

$$T = T_{st}\left[1 + \frac{\gamma - 1}{2}M^2\right] \tag{6}$$

The particle at the inlet with total temperature of 300 K and Mach number equal to 1.02 will have static temperate of 248 K, which is less than particle at core having static temperature of 256 K with total temperature of 270 K and Mach number equal to 0.5.

Radial profile of static and total temperature is plotted in Fig. 8. The decrease in static temperature in radial direction creates the temperature gradient for the heat energy to flow radially. This temperature gradient is maintained throughout the vortex tube length by the velocity gradient in radial direction. Radial velocity difference and hence static temperature gradient is maximum near inlet zone resulting in maximum heat transfer within the tube length of $L/D = 10$. However, by the action of shear created by the no slip boundary condition at the wall, static temperature increases radially very near to wall. In this region heat transfer will be in negative radial direction i.e. radially inwards. The magnitude of heat transfer has been discussed under Section 4.

4. Energy separation mechanism

Pressure at the inlet is the source of energy for energy separation in vortex tube. Core flow fluid particles are getting colder by loosing energy to peripheral flow particles. With this energy gain and conversion of kinetic energy to thermal energy by the action

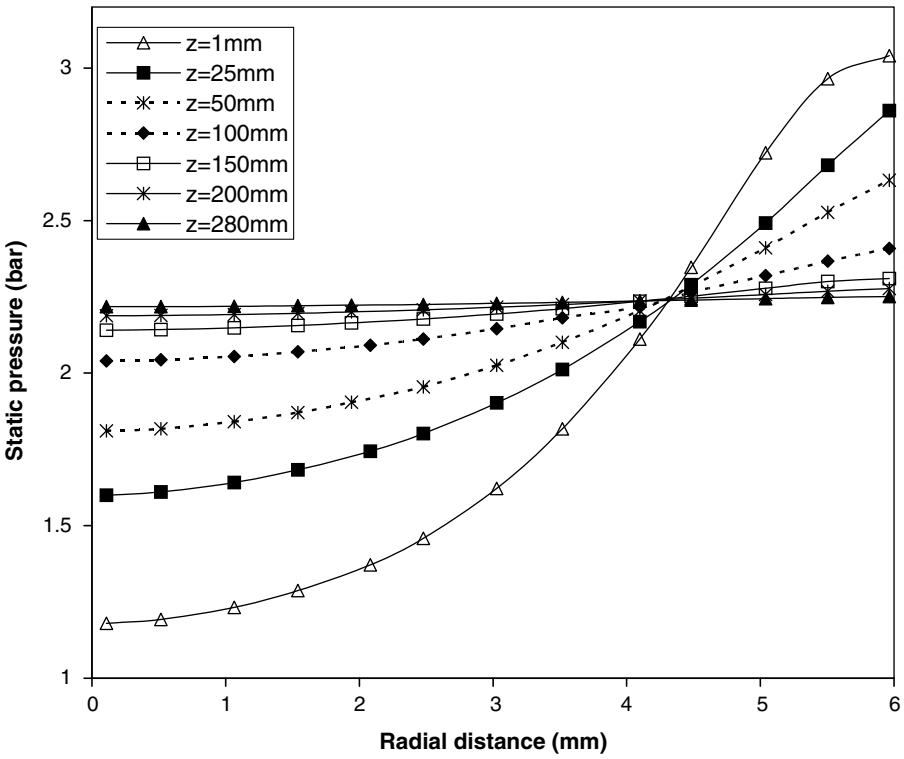

Fig. 6. Radial profile of static pressure.

of viscous shear, peripheral particles are getting heated up. Various theories have been proposed so far to explain this radial energy transfer. Secondary circulation flow proposed by Ahlborn and Groves [4,14] can not be the energy separation mechanism as discussed in our previous paper [13]. Contribution of acoustic streaming to energy separation [5] can be neglected as the energy separation phenomenon in our studies has been executed numerically with considerable agreement with experimental results without simulating acoustic streaming effect. Validity of intensive turbulent pulsation theory proposed by Hartnett and Eckert [15] is under serious doubt as the existence of free vortex zone in entire vortex tube can be discarded. In a very short span of time and length, free vortex becomes forced or quasi-solid vortex by the action of tangential stresses as stated by Gutsol [3]. Centrifugal separation of stagnant elements as stated by Gutsol is evident in vortex tube flow, but this does not contribute to radial energy transfer. A close look at the flow field and fluid property variation within the vortex tube will enlighten on the possible source for the radial energy transfer. It is evident from Fig. 9 that the angular velocity decreases radially outwards. This velocity gradient will lead to the transfer of work from fast moving layers to the slow moving layers i.e from inner layers to the peripheral layers in this case. This is in conformity with the observation of Aljuwayhel et al. [7] and supports the original energy separation theory proposed by Hilsch [2] wayback in 1947.

It can be seen from Fig. 8 that, the static temperature decreases radially i.e inner core flow layers are at higher static temperature than the peripheral layers except very near to the wall. This static temperature gradient leads to the transfer of heat from higher static temperature region to the lower static temperature region.

Though the magnitude of axial velocity is small compared to swirl velocity, it cannot be completely ignored. Axial velocity increases radially as shown in Fig. 3b, resulting in some work transfer from peripheral layers to their inner layers by the action of viscous shear.

To calculate the magnitude and direction of heat and work transfer, the flow field needs to be divided into two control volumes, a cold end exit flow region and a hot end exit flow region. Assuming the flow is axi-symmetric, the stream function can be defined as

$$\psi = \int_0^r \rho w r_b \mathrm{d}r \tag{7}$$

Streamlines for the three-dimensional model has been plotted using contour plot of stream function as show in Fig. 10. The dividing stream line is shown in Fig. 10b. The fluid outside this stream line flows through the hot flow exit and that inside is flows through the cold flow exit. Hence the transfer of energy across this stream line should give the energy transfer between the cold and the hot streams. The energy transfer takes place due to the shear work and heat transfer and these can be obtained by integrating the corresponding energy of line normal to the stream line over the dividing stream surface.

The magnitude of work transfer across the control volume boundary is given as

$$W = \int \int_{\Omega} \tau_{r\theta} = 2\pi\mu r_b^2 u \frac{\mathrm{d}\omega}{\mathrm{d}x} \tag{8}$$

where Ω is the surface of revolution of the dividing stream line.

Direction of heat flux depends on the location of the control volume boundary. If it lies within the boundary layer where static temperature increases radially then heat flux will be directed towards axis and if the thickness of hot flow region is thick enough to keep the boundary of control volume outside the boundary layer then heat flux will be radially outwards. Magnitude of heat flux across the control volume is calculated by following equation.

$$Q = \int \int_{\Omega} Q = 2\pi K_{\mathrm{eff}} r_b \frac{\mathrm{d}T}{\mathrm{d}x} \tag{9}$$

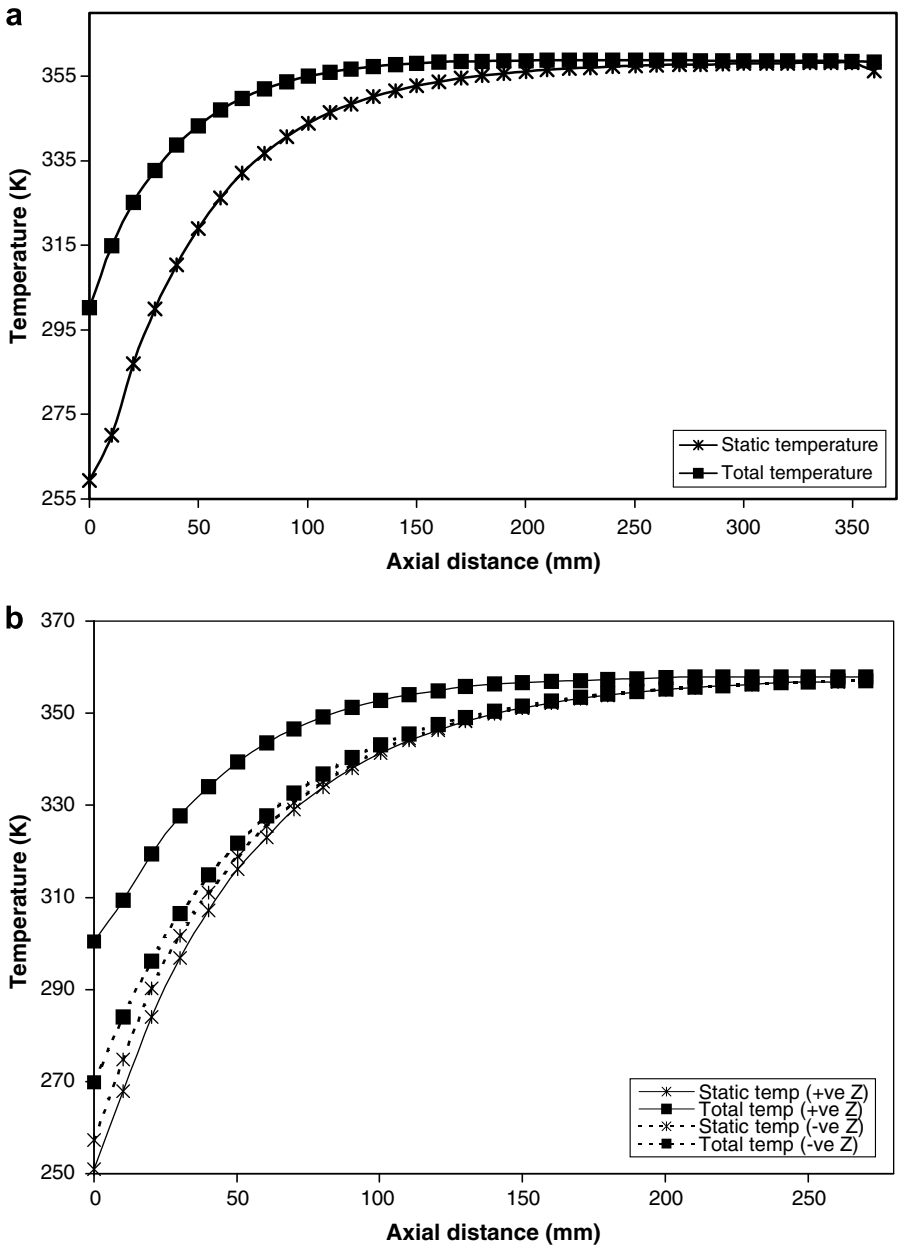

Fig. 7. Temperature of the tracked particle as it progresses in flow field: (a) particle exiting through hot end, (b) particle exiting through cold end after flow reversal (+ve Z: particle moving in +ve Z-direction, −ve Z: particle moving in −ve Z-direction).

Turbulent conductivity is calculated by equation

$$K_t = \frac{\mu_t C_p}{P_t} \tag{10}$$

Work transfer due to shear stress in axial direction is calculated with following equation.

$$W = \int\int_{\Omega} \tau_{rz} = 2\pi\mu r_b w \frac{dw}{dx} \tag{11}$$

Radial shear stress contribution to the total energy transfer can be neglected because of its minimal magnitude.

Rate of energy transfer for vortex tube with $L/D = 10$ has been shown in Fig. 11. The energy separation in vortex is due to predominant contribution of work transfer due to viscous shear in tangential direction. Work transfer due to viscous shear in axial direction in negative region indicates the work transfer has been from hot flow to cold flow. Heat transfer across the control volume boundary is in negative zone except very near to inlet. This is because of smaller thickness of hot flow, the control volume boundary is within boundary layer where the static temperature increases radially. Magnitude of energy transfer in vortex tube of $L/D = 10$ and 30 are given in Table 1. Energy separation from CFD model has been calculated using the equation

$$E = m_h h_h - m_h h_i \tag{12}$$

The calculated magnitude of energy transfer using Eqs. (8), (9) and (11) is in conformation with the CFD results.

As seen from Fig. 11, rate of work transfer due to viscous shear in tangential direction does not cease to zero within the tube length of $L/D = 10$. A longer vortex tube with $L/D = 30$ has been examined to cover the additional work transfer taking place beyond $10D$ length. Rate of energy transfer along axial distance is shown in Fig. 12 for $L/D = 30$. As seen from the figure the stagnation

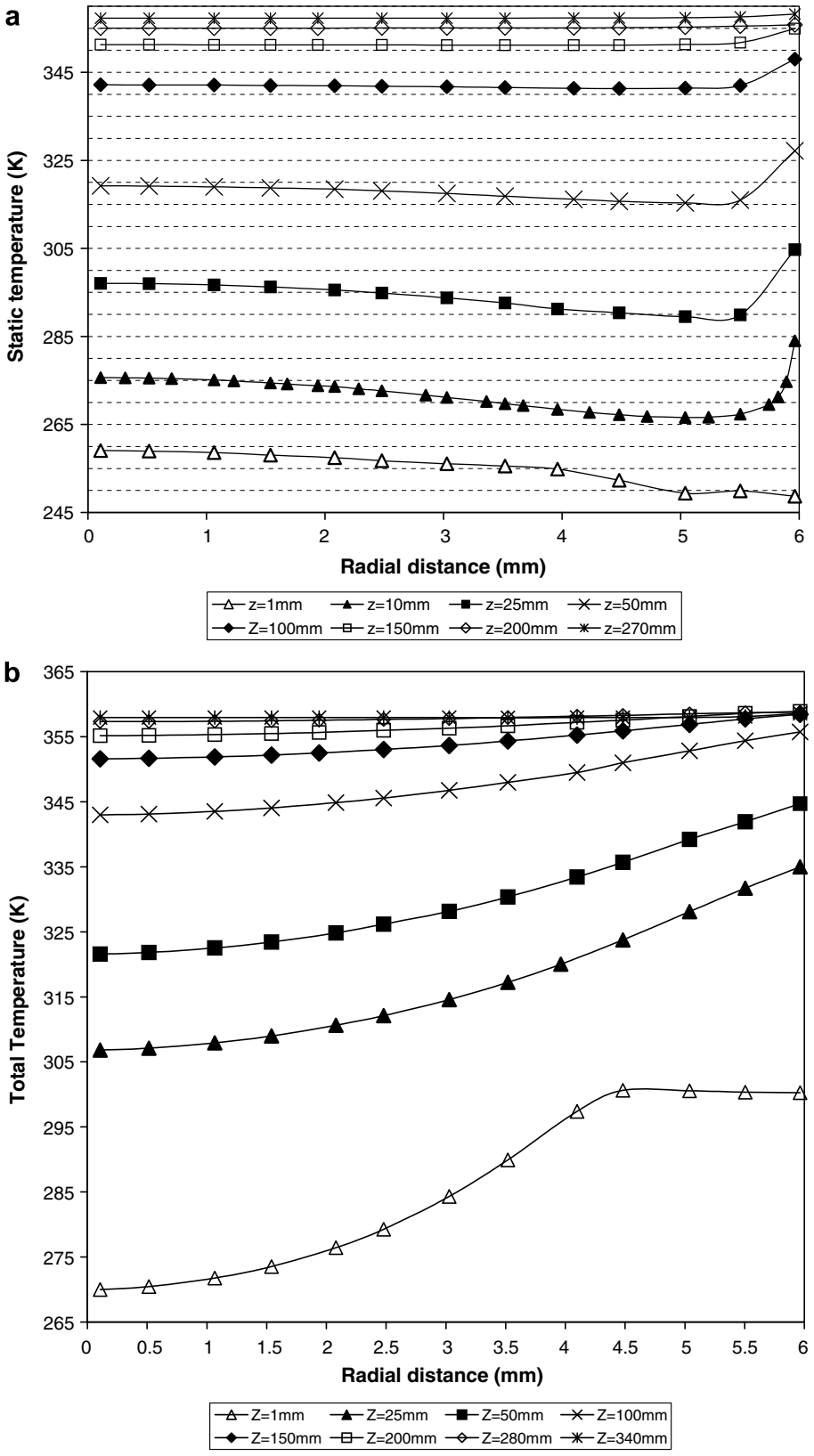

Fig. 8. (a) Radial profile of static temperature and (b) radial profile of total temperature.

point lies at a distance of about 240 mm from the inlet. The increased length has contributed to additional energy transfer of about 25% as shown in Table 1. The difference between calculated net energy transfer and the energy transfer computed by CFD model could be because of the neglected radial shear stress contribution to the total energy transfer.

To reduce the negative heat flux and hence increase the efficiency of vortex tube, vortex tube with higher hot gas fraction have

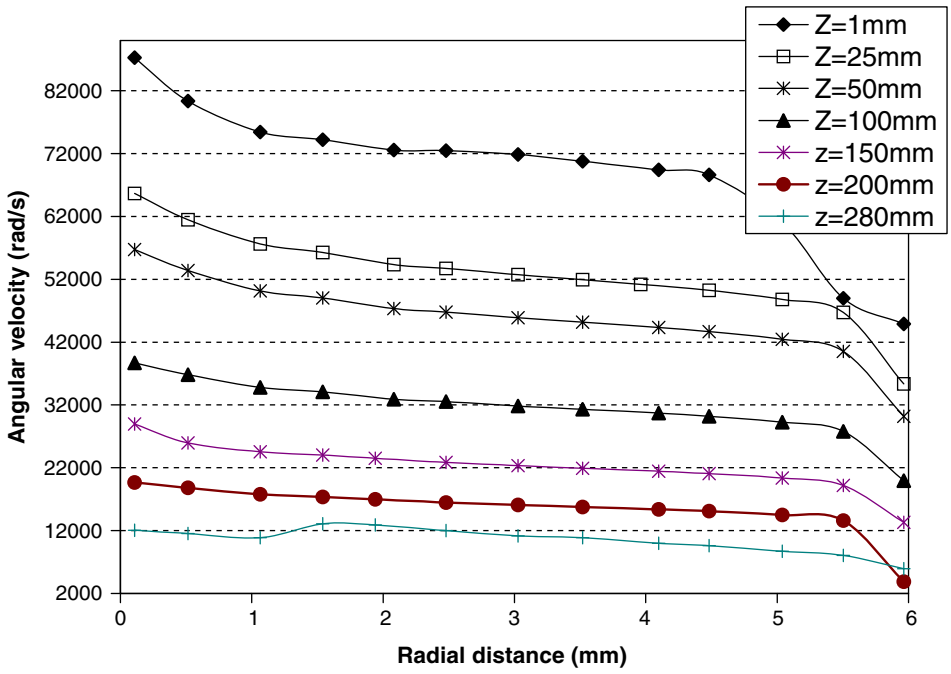

Fig. 9. Radial profile of angular velocity.

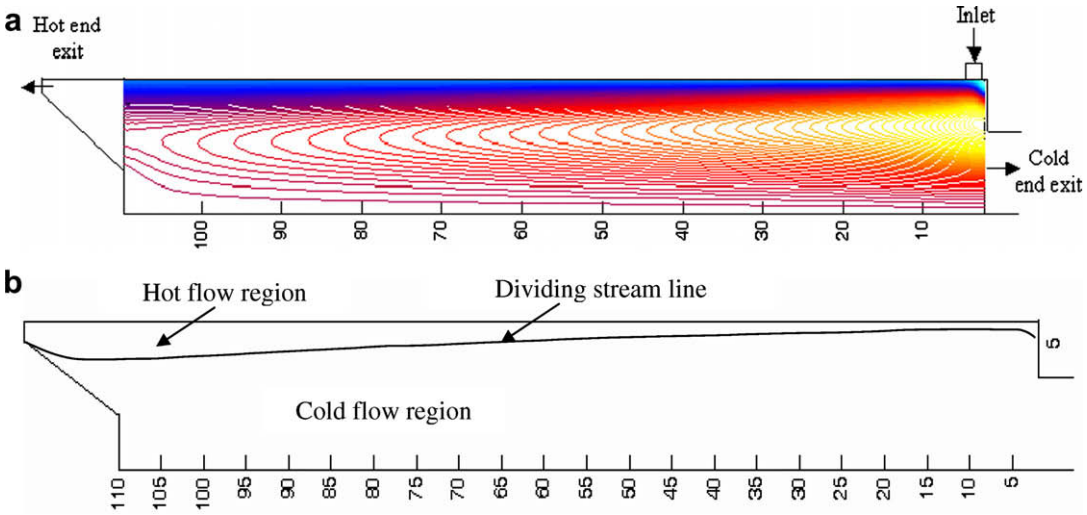

Fig. 10. (a) Streamline plot and (b) control volume boundary.

been analyzed so as to increase the thickness of hot gas region and bring the control volume boundary outside the boundary layers. Model with smaller number of cells have been used for these studies to reduce the time taken for computational analysis. This will lead to values of smaller magnitude of energy transfer than actual but are sufficient for a comparative study. Rate of energy transfer for hot end mass fraction of 15%, 26% and 35% have plotted in Fig. 13a–c for comparison. As seen from figures, the heat flux line has shifted into positive zone for higher hot mass fraction except near inlet zone. The magnitude of heat and work transfer is given in Table 2. As a result of significant reduction of negative heat transfer, the total energy separation has increased considerably. This explains the increase of efficiency of vortex tube at higher hot gas fraction. Most of the energy transfer is taking place within first 100 mm of the tube as seen from the rate of energy transfer plot which matches well with the temperature plot of the tracked particle in Fig. 7. Rate of energy transfer reduces away from the inlet and cease to zero at stagnation point. Difference between calculated net energy transfer and the energy transfer computed by CFD model is found to be more at higher hot gas fraction because of the increased negative energy transfer by radial velocity component, as the control volume boundary will not remain parallel to tube wall at higher hot gas fraction.

A degrading factor for the vortex tube performance is the secondary circulation flow which critically depends on the cold end diameter [13]. It has been shown [13] that for a 12 mm diameter vortex tube with $L/D = 30$, cold end diameter of 5 mm produces secondary circulation flow whereas the secondary circulation flow is completely eliminated for $d_c = 7$ mm. Experimentally it has been shown that the above dimension vortex tube produces a temperature difference between the hot and cold end exit of 94 K for $d_c = 5$ mm and 123 K for $d_c = 7$ mm [13]. The magnitude of heat

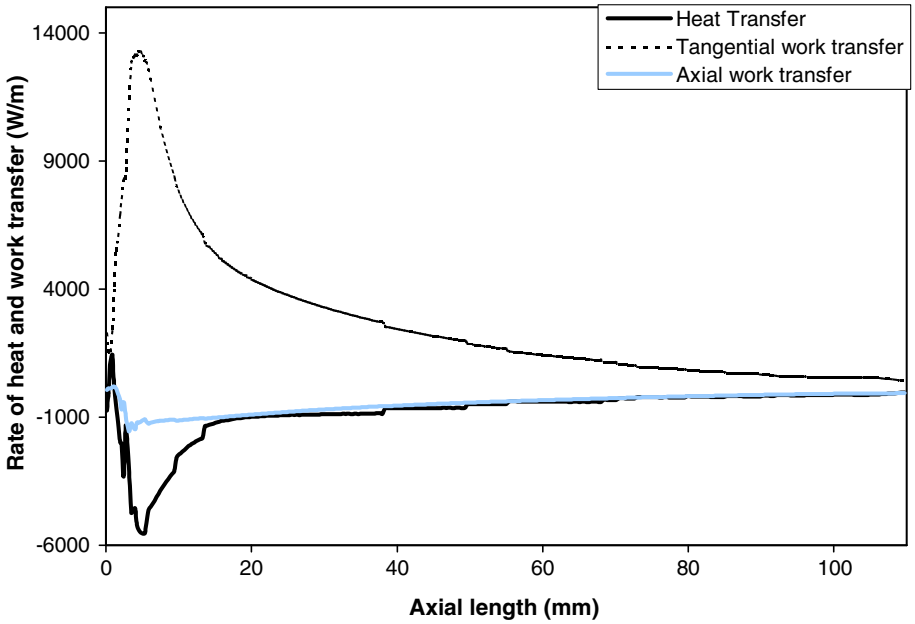

Fig. 11. Rate of energy transfer for $L/D = 10$, $d_c = 7$ mm, hot end flow = 26%.

Table 1
Magnitude of energy transfer for straight vortex tube with $D = 12$ mm, $d_c = 7$ mm and hot end flow = 30%

L/D ratio	Tangential work work transfer (W)	Axial work transfer (W)	Heat transfer (W)	Net energy transfer (W)	Energy transfer by CFD model (W)
10	295.477	−50.57	−85.039	159.87	154.2
30	297.898	−47.017	−51.01	199.87	192.3

and work transfer for cold end diameters of 5 mm and 7 mm for different hot gas fractions are shown in Table 2. The net energy transfer is around 82 W for $d_c = 5$ mm when compared to 104 W for $d_c = 7$ mm for the same vortex tube of $L/D = 10$ and hot gas fraction of 35%. It is observed that the existence of secondary circulation flow (for cold end diameter of 5 mm) has reduced the total energy transfer by about 21%.

5. Conclusion

A three-dimensional numerical model of Ranque–Hilsch vortex tube has been developed to analyze the flow parameters and energy separation mechanism inside the tube. An attempt has been made to investigate the variation of fluid properties and flow parameters as the fluid particles progress in the flow field by tracking different particles exiting through the hot and cold end.

- For the hot end exiting fluid particles, the swirl and axial velocities are maximum in the flow inlet zone and at this zone, swirl velocity is about 6 times higher than the axial velocity. For the

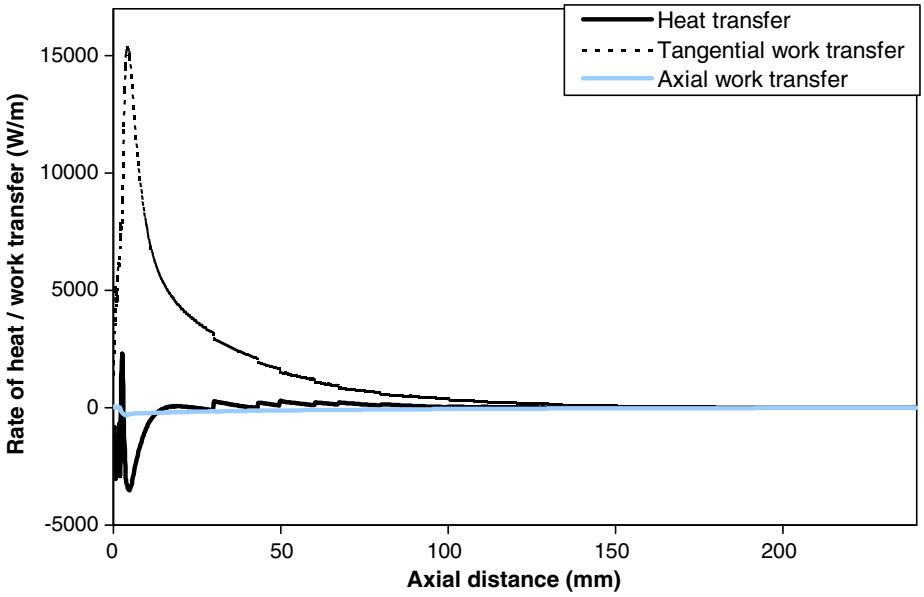

Fig. 12. Rate of energy transfer for $L/D = 30$, $d_c = 7$ mm, hot end flow = 30%.

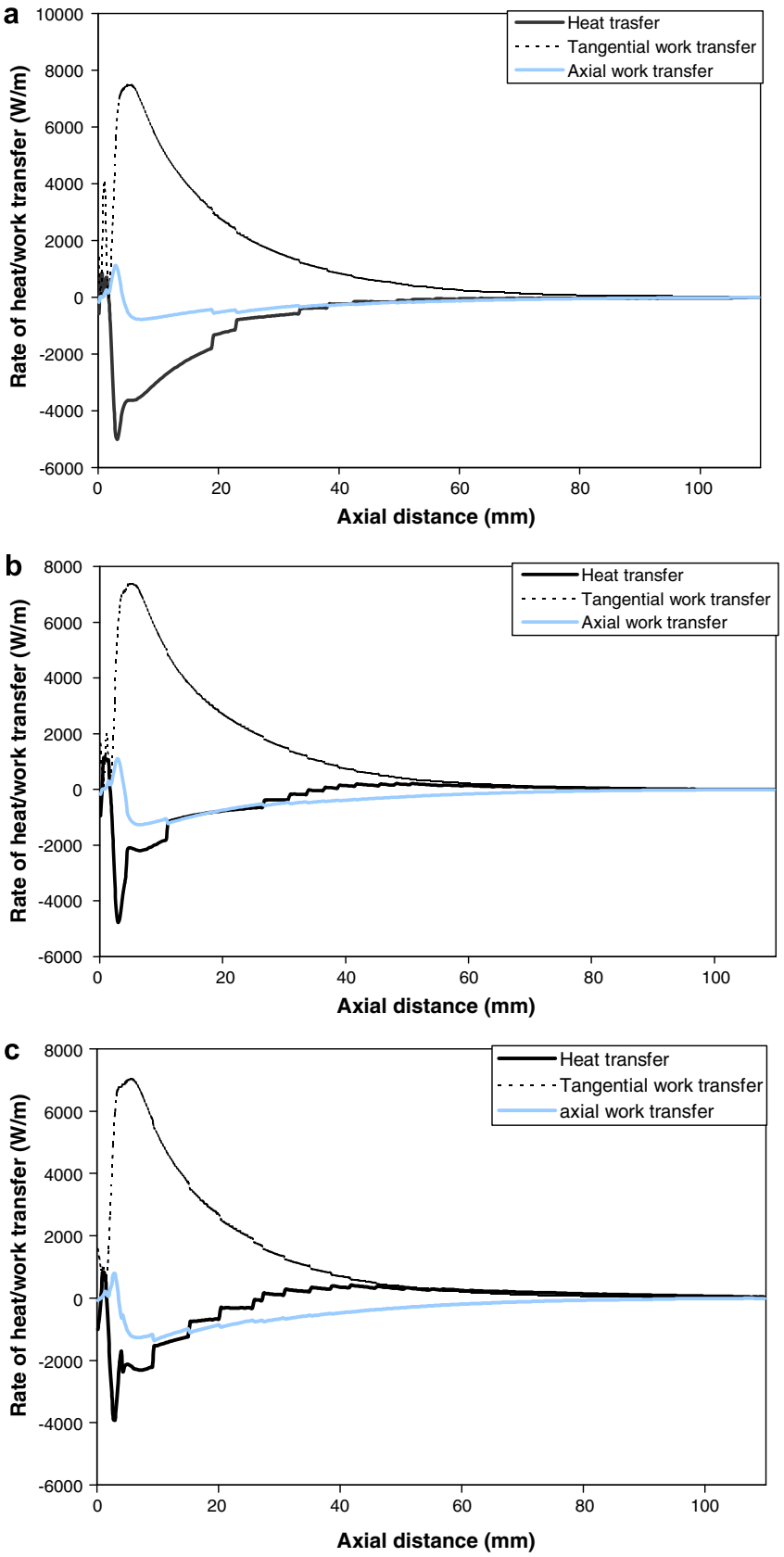

Fig. 13. Rate of energy transfer for $L/D = 10$, $d_c = 7$ mm: (a) hot end flow = 15%, (b) hot end flow = 26% and (c) hot end flow = 35%.

cold end exiting fluid particles up to the stagnation point, the swirl and the axial velocity profiles are similar to those of the hot end exiting fluid particles. However, from stagnation point, where the axial velocity becomes zero, its value increases to substantially higher values as the flow is accelerated by pressure difference between the flow field and cold end exit.

Table 2
Magnitude of energy transfer for straight vortex tube with $L/D = 10$, $D = 12$ mm

Cold end diameter (mm)	Hot end flow (%)	Tangential work transfer (W)	Axial work transfer (W)	Heat transfer (W)	Net energy transfer (W)	Energy transfer by CFD model (W)
7	15	141.65	−21.42	−66.93	53.30	52.27
7	26	134.85	−26.19	−32.79	75.87	77.64
7	35	131.35	−28.12	−11.59	91.63	104.40
5	35	128.64	−27.49	−20.71	80.43	82.00

- The swirl velocity profiles in the radial direction at different axial lengths show that the flow in the vortex tube is largely governed by the forced vortex regime, except at inlet zone which has a free vortex regime. This is contrary to the general perception that in Ranque–Hilsch vortex tube, the entire peripheral flow is free vortex and the core flow is forced vortex.
- There is a large drop in the static pressure in the nozzle, giving rise to nearly sonic velocity of the particles exiting the nozzle and thereafter only marginal reduction in static pressure up to stagnation point. However, both the static and total pressure decreases near to atmospheric pressure during the fluid flow from stagnation point to cold end exit.
- The lowest static temperature in the vortex tube is at the nozzle exit. Thereafter the static temperature for both the flow towards hot and cold end exits increases substantially in the first 10D length of the vortex tube and eventually reaches the value of the total temperature at the stagnation point. This can be attributed to the conversion of kinetic energy to thermal energy by the action of viscous shear forces. Thus there is no cooling process taking place in the vortex tube up to the stagnation point when moving from the inlet towards the hot exit even for a particle exiting from the cold end.
- For the fluid particles moving from the stagnation point towards the cold end exit, there is significant drop in static and total temperatures due to the energy transfer to peripheral particles.
- At any axial location, the static temperature of the fluid particles moving towards stagnation point is less than the static temperature of the particle on its travel from the stagnation point to cold end exit except at the inlet zone. This sets up the direction of heat transfer between the core and the peripheral flow in vortex tube.
- It is observed that in vortex tubes the angular velocity of the particles decreases radially outwards. This angular velocity gradient between the fast moving inner layers and the slow moving peripheral layers sets up energy transfer due to the action of viscous shear, resulting in the cooling of the core flow exiting through cold end.
- Since axial velocity of core flow increases radially, this sets up a counter acting energy transfer of viscous shear from peripheral layers to inner layers, though of lesser magnitude.
- Net energy transfer analysis involving tangential work transfer, axial work transfer and heat transfer through control volume analysis shows that by increasing the L/D ratio from 10 to 30 for the vortex tube investigated, the net energy transfer could be increased by about 25%, primarily due to decrease in heat transfer from peripheral to core flow.
- The higher thermal efficiency of vortex tube at higher hot gas fraction is due to substantial reduction in the negative heat transfer.
- For the same vortex tube and at the same hot gas fraction, an improper cold end diameter sets up secondary circulation flow and results in the reduction of energy transfer. By optimizing the cold end diameter higher energy transfer can be achieved in vortex tubes.

References

[1] G.J. Ranque, Experiences sur la detente giratoire avec productions simultanes d'un echappement d'air chaud et d'un echappement d'air froid, J. Phys. Radium 4 (7) (1933) 112–114.
[2] R. Hilsch, The use of the expansion of gases in a centrifugal field as cooling process, Rev. Sci. Instrum. 18 (2) (1947) 108–113.
[3] A.F. Gutsol, The Ranque effect, Phys.-Usp. 40 (6) (1997) 639–658.
[4] B. Ahlborn, S. Groves, Secondary flow in vortex tube, Fluid Dyn. Res. 21 (1997) 73–86.
[5] M. Kurosaka, Acoustic streaming in swirl flow and the Ranque–Hilsch (vortex-tube) effect, J. Fluid Mech. 124 (1982) 139–172.
[6] W. Frohlingsdorf, H. Unger, Numerical investigations of the compressible flow and the energy separation in Ranque–Hilsch vortex tube, Int. J. Heat Mass Transfer 42 (1999) 415–422.
[7] N.F. Aljuwayhel, G.F. Nellis, S.A. Klein, Parametric and internal study of the vortex tube using CFD model, Int. J. Refrig. 28 (2005) 442–450.
[8] H.M. Skye, G.F. Nellis, S.A. Klein, Comparison of CFD analysis to empirical data in a commercial vortex tube, Int. J. Refrig. 29 (2006) 71–80.
[9] S. Eiamsa-ard, P. Promvonge, Numerical investigation of the thermal separation in a Ranque–Hilsch vortex tube, Int. J. Heat Mass Transfer 50 (2007) 821–832.
[10] Star-CD, Version 3.10A: Methodology and User Guide, Computational Dynamics Limited, UK, 1999.
[11] V. Yakhot, S.A. Orszag, Renormalization group analysis of turbulence – I: Basic theory, J. Sci. Comput. 1 (1986) 1–51.
[12] T. Farouk, B. Farouk, Large eddy simulations of the flow field and temperature separation in the Ranque–Hilsch vortex tube, Int. J. Heat Mass Transfer 50 (2007) 4724–4735.
[13] U. Behera, P.J. Paul, S. Kasthurirengan, R. Karunanithi, S.N. Ram, K. Dinesh, S. Jacob, CFD analysis and experimental investigations towards optimizing the parameters of Ranque–Hilsch vortex tube, Int. J. Heat Mass Transfer 48 (2005) 1961–1973.
[14] B. Ahlborn, J.U. Keller, R. Staudt, G. Treitz, E. Rebhan, Limits of temperature separation in a vortex tube, Phys. D: Appl. Phys. 27 (1994) 480–488.
[15] J.P. Hartnett, E.R.G. Eckert, Experimental Study of the Velocity and Temperature Distribution in a High-Velocity Vortex-type Flow, Publication of Heat Transfer Laboratory, University of Minnesota, Minneapolis, 1956.